An Unconstrained Architecture for High-Order ΣΔ Force-Feedback Inertial Sensors

J. Raman, P. Rombouts and L. Weyten

Ghent University (UGent), Dept. ELIS, Sint-Pietersnieuwstraat 41, 9000 Ghent, Belgium

***Abstract*— ΣΔ force-feedback loops have to deal with a stability problem due to phase-lag occurring in the sensor. To tackle this problem traditionally a compensator is introduced in the loop. We show that this traditional approach imposes a constraint on the realizable NTF such that the NTF cannot be optimized. Next we propose a novel unconstrained architecture that allows to implement any NTF. This way greatly improved quantisation noise shaping can be obtained. In a typical design example the improvement was 12 dB**

I. Introduction

The concept of ΣΔ force-feedback for inertial sensors, has many benefits [1]–[6]. It is a closed-loop approach where the inertial force is counterbalanced by a single-bit feedback force. Due to this, it has the possibility of improving bandwidth, increasing dynamic range, and reducing sensitivity to process and temperature variations of the mechanical transfer. Next to this, the use of bi-level actuation in the feedback path provides a good overall linearity. Last but not least, the inherent A/D conversion is important for easy downstream processing of the sensor data.

From a designer's point of view, ΣΔ force-feedback loops are more difficult to design as purely electrical ΣΔ modulators. The main problem is an inherent stability problem which originates from the fact that the mechanical sensor behaves as a second order mass-damper-spring system. Put explicitly, the relation between the force acting on the proof mass and the resulting displacement is given by:

$$T_{mech}(s) = \frac{1/k}{1 + \frac{1}{Q}\frac{s}{\omega_0} + \left(\frac{s}{\omega_0}\right)^2} \tag{1}$$

In this, k denotes the spring constant, Q the quality factor and $\omega_0/(2\pi)$ the resonant frequency. An equivalent system-level representation of the mechanical sensor is shown in fig. 1. Its main signal path contains two integrations. Unfortunately, the inner node (corresponding to the speed v of the proof mass) is not directly accessible. When used within a ΣΔ feedback loop, the mechanical system contains — roughly speaking — "one integration too much", which causes problems with respect to the stability of the loop. In literature, control-theory-based solutions have been proposed to stabilize the loop [1]–[5]. These approaches consist of adding a compensating filter with some differentiating action to the loop. Typically, a first order FIR filter such as $2–z^{-1}$ is used. Unfortunately, this compensator also introduces extra poles in the loop (here at $z = 0$) and affects the noise-shaping performance of the ΣΔ system. As a result, the relation between stability and performance of the ΣΔ loop gets cluttered, making it difficult to optimize the trade-off between them.

II. Traditional architectures

A. Architectural structure

The typical architecture for a ΣΔ force-feedback is largely inspired on electrical ΣΔ modulators. We illustrate this by means of a fifth-order discrete time electrical modulator displayed in fig. 2. In this

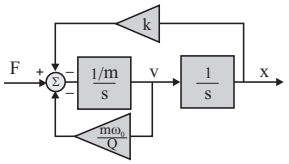

Fig. 1. System-level diagram of the mechanical sensor, which behaves as a second order mass-damper-spring system.

architecture, full control of the noise transfer function (NTF) poles is obtained by direct observation of all integrator states: the NTF-poles can be placed at arbitrary positions through the five coefficients a_i. The coefficients γ_j are used to set the zeros of the NTF at the optimized positions within the passband.

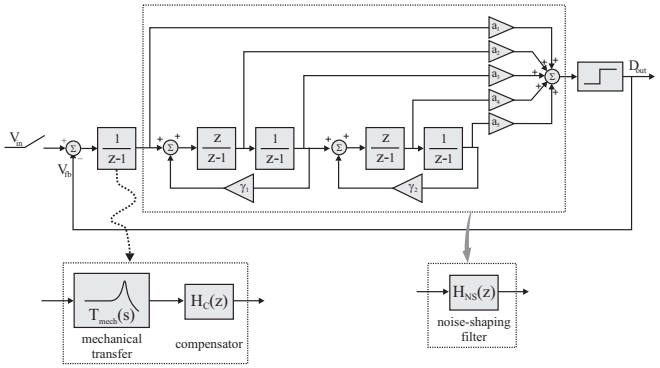

Fig. 2. Conceptual steps in converting a feedforward type electrical ΣΔ modulator to a single-feedback force-feedback architecture.

To convert this structure to a mixed mechanical-electrical architecture, we conceptually isolate the first integrator and replace it with the mechanical transfer. However, as already explained in the introduction, in comparison with the replaced integrator, the mechanical transfer contains two integrations. From the transfer of eq. (1) it can easily be seen that for frequencies above the resonant frequency phase-lags of up to 180° occur. The traditional approach to deal with this is to add a compensation filter with differentiating action to introduce enough phase-lead to stabilize the system. Therefore, for reasons of stability, the first integrator of fig. 2 is replaced by the mechanical transfer and this compensation filter $H_C(z)$.

The rest of the ΣΔ integrator stages of fig. 2 can be thought of as an (electrical) filter $H_{NS}(z)$. We will call this the noise-shaping filter. This additional filter $H_{NS}(z)$ is needed to improve the quantisation noise shaping [3]. It can readily be seen that the position of the filters $H_C(z)$ and $H_{NS}(z)$ can be exchanged without affecting the system behavior. Finally, the loop contains a one-bit quantizer which outputs

the digital value D_{out}, which has two possible values: ± 1.

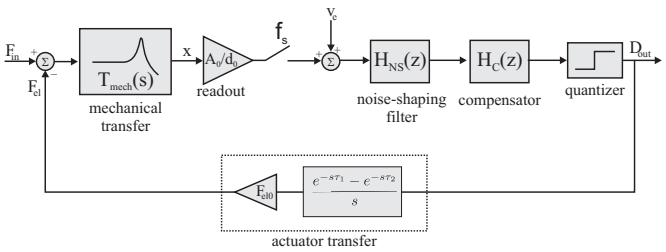

Fig. 3. Single-feedback $\Sigma\Delta$ force-feedback loop.

Until now, the introduced transformations have been conceptually. In reality, we also need to take care of the proper domains (mechanical/electrical) in which the different transfer functions take place and introduce the interfacing steps explicitly. This is shown in fig. 3, where two extra blocks can be noted. First, a readout circuit is present, translating the mechanical displacement into a sampled output voltage. Second, we also have the actuator translating the one-bit digital output to a bi-level actuation force-pulse used for mechanical feedback.

Let us first look at the readout circuit. Typically a differential capacitive readout interface is used, based on measuring the relative magnitude of two parallel-plate sensing capacitors C_{s+} and C_{s-}:

$$C_{s+} = \frac{C_{s0}}{1 - x/d_0} \qquad C_{s-} = \frac{C_{s0}}{1 + x/d_0}$$

In this, C_{s0} denotes the zero-displacement capacitance. We see that these capacitances change as a function of the normalized displacement x/d_0. Hence, the readout circuit delivers an output voltage proportional to the normalized displacement (to first order). We assume that, by design, the bandwidth of the readout circuit is high enough to represent this as a simple scale factor A_0. Therefore, the transfer from displacement x to the readout voltage reduces to a mere factor A_0/d_0. In the diagram, the sampling operation is placed after the readout gain. Frequently, readout circuits based on switched-capacitor techniques are used [2], [5]. While these circuits directly generate sampled outputs, they can still conceptually be represented by a continuous-time readout followed by an explicit sampling operation, as shown in fig. 3. Therefore, both cases are covered by this system-level diagram.

With respect to the feedback path, we assume the possibility to generate a constant actuation force F_{el0} in either the positive or the negative direction. The direction of the feedback force is determined by the digital output D_{out}, which assumes values $+1$ or -1. In the simplest case, the feedback force is applied during an entire sampling period. In practice, this requires the use of separate capacitors for actuation. If the same set of capacitors is multiplexed in time for both readout and actuation, the actual time interval available for force-feedback is smaller than one full sampling interval $[0, T]$. Therefore, we consider the more general case where the feedback force is applied for a time interval $[\tau_1, \tau_2]$, with $0 \leq \tau_1 < \tau_2 \leq T$. We then have the following s-domain relation that represents actuation:

$$F_{el}(s) = F_{el0} \frac{e^{-s\tau_1} - e^{-s\tau_2}}{s} D_{out}(z)|_{z=e^{sT}}$$

This is also shown on the system-level diagram of fig. 3.

We now want to examine the noise-shaping properties of this $\Sigma\Delta$ force feedback loop with respect to quantization noise. This is represented by the discrete-time transfer NTF(z). Note however, that the system of fig. 3 contains both continuous-time and discrete time blocks. In order to extract the NTF, we first calculate the equivalent discrete-time transfer function from the digital output D_{out} to the sampled readout voltage.

B. Equivalent discrete-time loop transfer

Combining the transfers from the (actuation) pulse shaper, the mechanical system and the readout circuit, we obtain the continuous-time transfer:

$$T_c(s) = \frac{e^{-s\tau_1} - e^{-s\tau_2}}{s} \frac{M_0}{1 + 2\cos\theta \frac{s}{\omega_0} + \left(\frac{s}{\omega_0}\right)^2} \tag{2}$$

with $M_0 = \frac{F_{el0}}{k \cdot x_0}$. Note that we have introduced a "damping angle" $\theta = \arccos(1/(2Q))$ as a measure of the quality factor of the mechanical system. With this notation, the (complex conjugate) mechanical poles s_m and s_m^* have the following simple expression:

$$s_m = -\omega_0 \, e^{+j\theta} \qquad s_m^* = -\omega_0 \, e^{-j\theta} \tag{3}$$

The equivalent discrete-time transfer obtained from sampling $T_c(s)$ is given by (detailed calculations are omitted for compactness):

$$T_d(z) = \frac{R_0}{z - z_m} + \frac{R_0^*}{z - z_m^*} \tag{4}$$

with

$$R_0 = \frac{M_0 \, e^{-j\theta}(e^{-s_m\tau_1} - e^{-s_m\tau_2})z_m}{2j \sin\theta}$$

In this, z_m and z_m^* represent the discrete-time poles corresponding to the mechanical system. These poles are related to the continuous-time mechanical poles through the mapping e^{sT}, that is $z_m = e^{s_m T}$ and $z_m^* = e^{s_m^* T}$. We see that, next to two complex conjugate mechanical poles, $T_d(z)$ also has a zero:

$$z_z = \frac{R_0 \, z_m^* + R_0^* \, z_m}{R_0 + R_0^*} \tag{5}$$

With the equivalent discrete-time transfer function $T_d(z)$, it is very easy to write down the discrete-time loop filter $H(z)$ of the $\Sigma\Delta$ force-feedback architecture of fig. 3:

$$H(z) = T_d(z) H_C(z) H_{NS}(z) \tag{6}$$

Now we will examine the corresponding NTF and show that the architecture imposes a (hidden) constraint.

C. Constrained NTF of traditional architectures

As is common, we approximate the 1-bit quantizer as an additive quantisation noise source with an approximate linear (noise) gain G_n [7]. With this, the expression for NTF(z) becomes:

$$\text{NTF}(z) = \frac{1}{1 + G_n \, H(z)} \tag{7}$$

It is especially useful to look at the NTF in factored form. Let us first consider the case when no compensator is present ($H_C(z) \equiv 1$). Then, within the loop we have an electrical filter $H_{NS}(z)$ of order $N-1$ and a mechanical transfer $T_d(z)$ of order two, resulting in a system of order $N+1$. Therefore, the NTF has $N+1$ zeros and an equal number of poles:

$$\text{NTF}(z) = \frac{\overbrace{(z - z_m)(z - z_m^*)}^{\text{mechanical}} \overbrace{(z - z_{ns,1}) \ldots (z - z_{ns,N-1})}^{\text{electrical noise-shaping}}}{(z - z_1)(z - z_2)(z - z_3) \ldots (z - z_{N+1})} \tag{8}$$

The primary objective of a $\Sigma\Delta$-system is to keep the quantization noise level low in the baseband. For this purpose, the NTF-zeros

play a crucial role. Here, in the electromechanical $\Sigma\Delta$, two complex conjugate zeros (z_m and z_m^*) due to the mechanical transfer are present. Typically, these NTF-zeros do not allow a very aggressive noise shaping. Especially for lower quality factors, z_m is located inside the unit circle, limiting its noise-shaping effect. Practical implementations confirm that in this case the performance is limited by quantization noise. For instance, the closed-loop performance of the sensor in [5] is up to ten times worse compared to open-loop operation. To overcome this, an electrical noise-shaping filter $H_{NS}(z)$ is needed to introduce extra NTF-zeros. By building this filter as a sequence of resonators (as in fig. 2), these zeros can be located on the unit circle at a position controlled by the local feedback factors γ_i. If these zeros are spread optimally over the baseband, a significant performance increase can be obtained [8].

Having placed the NTF-zeros such as to optimize baseband noise-shaping, we next turn to the stability of the $\Sigma\Delta$ system. It is widely known that the stability of higher-order $\Sigma\Delta$ systems requires a judicious choice of the NTF poles [8]. I.e., the $N+1$ NTF-poles ($z_1,\ z_2\ \ldots z_{N+1}$) must be placed appropriately. However, by inspection it is observed that the $\Sigma\Delta$ loop of fig. 3 only provides N degrees of freedom. Hence the $N+1$ NTF-poles cannot be placed at arbitrary positions. It even turns out that none of the realizable pole constellations provide enough system stability to be of practical value. This is reminiscent of the fact that the electrical $\Sigma\Delta$ of fig. 2 cannot be stable if for instance a_1 is zero.

As already explained, the tradtional way to deal with this stability problem is to add a compensation filter $H_C(z)$ to the loop. With an Mth order compensation filter, the NTF takes the form:

$$\mathrm{NTF}(z) = \frac{\overbrace{(z-z_m)(z-z_m^*)}^{\text{mechanical}}\overbrace{(z-z_{ns,1})\ldots(z-z_{ns,N-1})}^{\text{electrical noise-shaping}}}{(z-z_1)(z-z_2)(z-z_3)\ldots(z-z_{N+1})} \times \frac{\overbrace{(z-z_{C,1})\ldots(z-z_{C,M})}^{\text{compensator}}}{(z-z_{N+2})\ldots(z-z_{N+M+1})}$$

The M compensator poles ($z_{C,1},\ \ldots,\ z_{C,M}$) appear as extra zeros in the NTF. While the compensator increases the order of the loop, in general, the added NTF-zeros do not contribute to the baseband noise-shaping or, even worse, have a negative effect on the in-band noise. The only added value is that now the $N+M+1$ NTF poles can be placed at locations where we at least obtain a stable system. However, with N+M degrees-of-freedom for placing N+M+1 poles, the architecture still imposes an implicit constraint on the realizable NTF.

III. Unconstrained architecture

From the analysis above, we know that the traditional architectures lack one degree-of-freedom to allow arbitrary placement of NTF poles. We will now construct an unconstrained architecture, which has sufficient degrees-of-freedom to place the poles in a designed, stable position. It is obvious that this allows to remove the compensator filter.

In order to understand the principle, we refer to fig. 4. We start again from an unconstrained electrical architecture. Instead of focussing on the first integrator, we rather look at the front-side resonator stage (consisting of two integrators). As a first step, we convert the feedback path to the inner node of the first integrator to a feedforward path, as shown in fig. 4 (b). It is easy to see that that the transfers from X to Y for structures (a) and (b) are identical. This can be demonstrated by direct calculation, but it is also a direct consequence of the equivalence of a feedforward-type and a feedback-type $\Sigma\Delta$ modulators of second order. From this, we further deduce that the loop filters of structure (a) and (b) are equivalent. The next step is to displace the feedforward path of the first resonator stage to the right, resulting in fig. 4 (c). The equivalence of structures (b) and (c) can again be derived from the fact that the loop filters are identical. Since in structure (c) the signal at the inner node of the first resonator stage is not needed, it can be replaced by the mechanical resonator without loss of degrees-of-freedom. This way, we have demonstrated that by simply adding one feedforward path in a mixed-feedback architecture, an unconstrained $\Sigma\Delta$ force-feedback architecture can be obtained.

Note that, apart from the first resonator, other resonator stages in fig. 4 are of the feedback type. It can readily be demonstrated that the "construction method" equally applies if feedforward stages are present, provided that the feedback path to the input of the second stage is maintained (corresponding to coefficient a_3 in fig. 4).

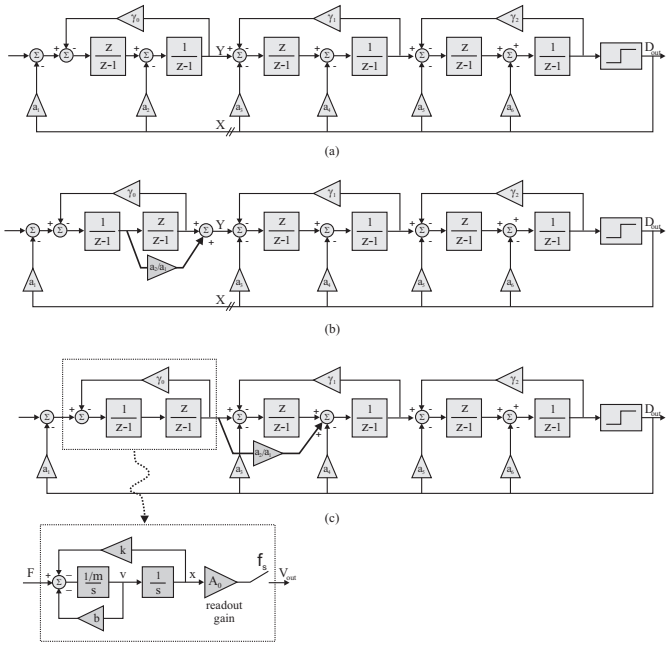

Fig. 4. Conceptual steps in converting an electrical $\Sigma\Delta$ modulator with partial feedforward and feedback to an unconstrained force-feedback architecture.

Because we now have knowledge of an unconstrained $\Sigma\Delta$ force-feedback architecture, we can follow an analogous design flow as used for purely electrical $\Sigma\Delta$ modulators [8], [9].

IV. Comparative Design Example

In order to illustrate the possibilities offered by the unconstrained architecture when it comes to quantization noise shaping, we work out a comparative design example. As a reference design, we take the single-feedback architecture of [3] for implementing a bandpass $\Sigma\Delta$ force-feedback loop. The resulting structure, shown in fig. 5 (a), can for instance be used for readout of the secondary mode of a gyroscope. Starting from the values $\tau_1 = 3/16$, $\tau_2 = 10/16$, $f_0 = 5$KHz, $f_s = 850$KHz, and assuming $Q = 5$ (not specified in [3]), the equivalent mechanical transfer $T_d(z)$ is given by

$$T_d(z) = 0.0016729\frac{z+0.6819}{(z-z_m)(z-z_m^*)} \qquad (9)$$

where z_m equals $0.99631\, e^{j2\pi 0.0058545}$. By choosing $\gamma = 2(1-\cos(\omega_0/f_s))$, the electrical filter is set to resonate also at the mechanical resonant frequency, which significantly improves the quantization noise shaping around this frequency. For exactly the same mechanical transfer T_d, also an unconstrained modulator structure is designed based on conventional design techniques for electrical $\Sigma\Delta$ modulators [8], [9]. The result (after rounding of some coefficients to convenient values) is shown in fig. 5 (b). Note that the scale factor of $T_d(z)$ in Eq. (9) was chosen based on the mixed-feedback design. This scale factor is controlled by the readout gain and is not important for the single-feedback architecture (and not specified in [3]).

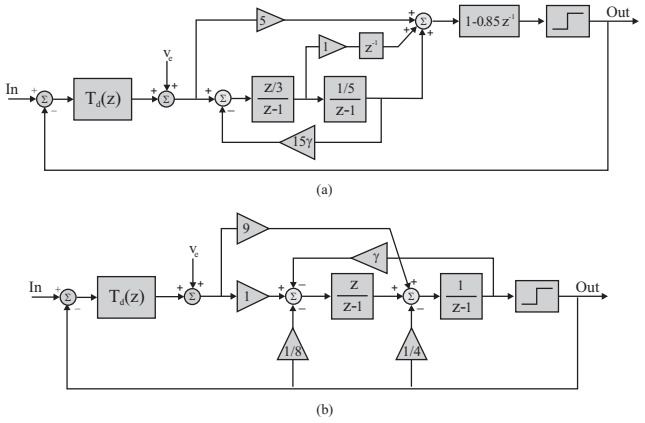

Fig. 5. Comparative design example: (a) original structure according to [3] and (b) unconstrained architecture.

Both structures have been simulated for the same sinusoidal input signal. The (averaged) output spectrum is displayed in fig. 6. Also shown is a theoretical prediction of this spectrum based on NTF(z). Clearly, the unconstrained architecture realizes a better shaping of quantization noise, resulting in an SNR improvement of 12dB.

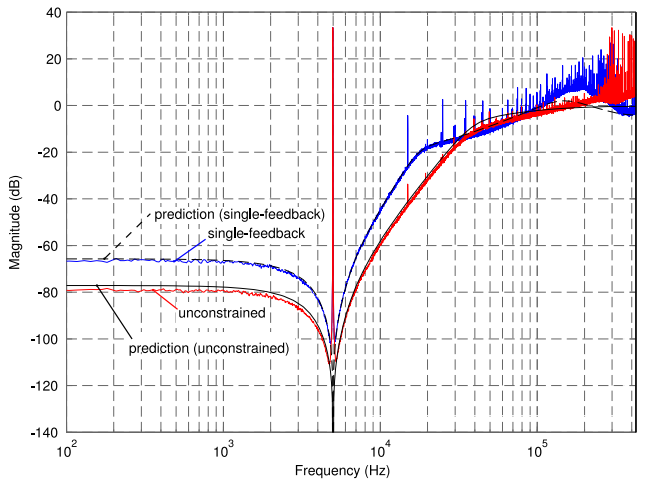

Fig. 6. Comparative design example: quantization noise shaping of the single-feedback architecture and the new unconstrained architecture.

V. Robustness to Parameter Variations

Because a one-bit quantizer only looks at the sign of its input signal, any change in the loop gain which can be modelled as a positive scale factor theoretically does not affect system stability. This implies that structures with only one feedback path (e.g. the traditional structure of fig. 5(a)) are very insensitive to variations of some parameters, e.g., the actuation voltage, the actuation capacitance, the readout capacitance (and in general the readout gain). The tolerances on these parameters are so large that it is possible to use the same single-feedback architectures with different sensors [3].

The unconstrained architecture has multiple feedback paths. The overall feedback is mechanical in nature, whereas the others are electrical in nature. Here, the relative strength of the mechanical path compared to the electrical path(s) influences the stability of the system. Therefore, the allowed tolerances on the above parameters are considerably less. This does not mean, however, that these tolerances are difficult to meet, as is also evidenced from prototype development [6]. Moreover, in practice, the stability of a mixed-feedback architecture can easily be tuned. The tuning principle relies on the fact that the stability of the system increases by strenghtening the electrical path(s). E.g., in a (switched-capacitor) implementation, this can easily be done by calibrating the reference voltage of the feedback DAC.

VI. Conclusions

We have shown that traditional $\Sigma\Delta$ force-feedback architectures cannot implement an arbitrary NTF, because they lack one degree of freedom. Moreover, these structures require a compensation filter in the loop to obtain an acceptable stable structure. In this manuscript, we have presented an unconstrained architecture by replacing the front-side resonator stage of an electrical $\Sigma\Delta$ modulator with the mechanical sensor in such a way that the signal at the inner node is not needed. This unconstrained architecture allows to implement any NTF, and hence does not require a compensator filter. Moreover, established design techniques for electrical $\Sigma\Delta$ modulators can now also be applied to $\Sigma\Delta$ force-feedback loops. We demonstrated that this way, greatly improved quantization noise performance can be obtained (in our design example 12 dB).

References

[1] X. Jiang, J. I. Seeger, M. Kraft, and B. E. Boser, "A monolithic surface micromachined Z-axis gyroscope with digital output," in *Symp. on VLSI Circuits Dig. Tech. Papers*, Honolulu, 2000, pp. 16–19.

[2] T. Kajita, U.-K. Moon, and G. Temes, "A two-chip interface for a MEMS accelerometer," *IEEE Transactions on Instrumentation and Measurement*, vol. 51, no. 4, pp. 853 – 858, aug 2002.

[3] V. P. Petkov and B. Boser, "A fourth-order $\Sigma\Delta$ interface for micromachined inertial sensors," *IEEE J. Solid-State Circuits*, vol. 40, no. 8, pp. 1602–1609, august 2005.

[4] Y. Dong, M. Kraft, C. Gollasch, and W. Redman-White, "A high-performance accelerometer with a fifth-order $\Sigma\Delta$ modulator," *J. Micromech. and Microeng.*, vol. 15, no. 7, pp. 22–29, July 2005.

[5] H. Külah, J. Chae, N. Yazdi, and K. Najafi, "Noise Analysis and Characterization of a Sigma-Delta Capacitive Microaccelerometer," *IEEE J. Solid-State Circuits*, vol. 41, no. 2, pp. 352–361, february 2006.

[6] J. Raman, E. Cretu, P. Rombouts, and L. Weyten, "A Digitally Controlled MEMS Gyroscope With Unconstrained Sigma-Delta Force-Feedback Architecture," in *Proc. 19th IEEE Int. Conf. on Micro Electro Mechanical Systems*, january 2006, pp. 710–713.

[7] S. H. Ardalan and J. J. Paulos, "An Analysis of Nonlinear Behavior in Delta-Sigma Modulators," *IEEE Trans. Circuits Syst.*, vol. 34, pp. 593–603, june 1987.

[8] R. Schreier, "An Emperical Study of Higher-Order Single-Bit Delta-Sigma Modulators," *IEEE Trans. Circuits Syst. II*, vol. 40, no. 8, pp. 461–466, August 1993.

[9] ——, *The Delta-Sigma toolbox for MATLAB*, Oregon State University, november 1999.